Journal of chemical & engineering data

Article

pubs.acs.org/jced

Effects of Electric Field on the Vapor−Liquid Equilibria of Nanoconfined Methanol and Ethanol

Debdip Bhandary, Kartik Srivastava, Rajat Srivastava, and Jayant K. Singh*

Department of Chemical Engineering, Indian Institute of Technology Kanpur, Kanpur-208016, India

ABSTRACT: The effects of the electric field on the vapor−liquid equilibria of methanol and ethanol confined in a graphitic slit pore of width 4 nm using molecular dynamics simulations are reported. The vapor−liquid critical temperature of methanol gets suppressed under confinement. The external electrical field further decreases the critical temperature with increasing electric field strength up to E = 1.5 V·nm^{-1}. Surprisingly, a further increase in the electric field strength reverses the critical temperature behavior and is seen to increase with increasing electric field. The reversible behavior of the critical temperature with the electric field is also seen for nanoconfined ethanol at approximately 1.5 V·nm^{-1}. The critical density, on the other hand, is found to continuously decrease with increasing electric field strength. Application of an external electric field results in the decrease in vapor and liquid densities. The coordination number in the liquid phase is found to decrease first with increasing electric field until E = 1.5 V·nm^{-1} and then increases with a further increase in the electric field, confirming the observed trend in the critical temperature according to the mean field theory. Orientational order of nanoconfined methanol and ethanol, on the other hand, is found to increase with increasing electric field.

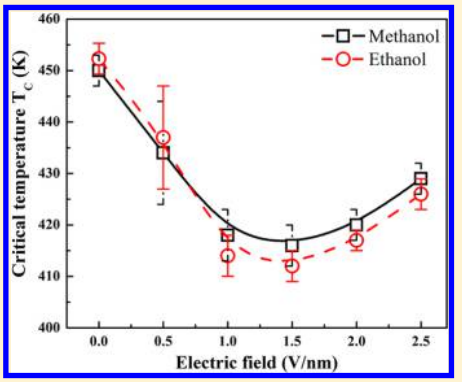

1. INTRODUCTION

The thermo-physical properties of fluids have been known to alter significantly at nanometer length scale due to surface effects.[1−9] Several studies have been conducted to study the effect of nanoconfinement on the vapor−liquid phase behavior of fluids, and contrasting results have been found as compared to those for the bulk fluids. The vapor−liquid phase transition undergoes a cross-over behavior from 3D to 2D phase transitions with reduction in the pore size.[9−12] The critical temperature decreases under confinement in general; on the other hand critical density nonmonotonically changes with confinement. Furthermore, fluid under extreme confinement is found to experience enormous anisotropic pressure[11], of the order of 10^3−10^5 bar, with the tangential component two orders higher than the normal component.

Understanding the properties of confined fluids is necessary to create efficient new technologies, such as molecular detection,[14] gas storage,[15] and membrane separation.[16,1718] Another such example is the mechanism proposed by Ge et al.[19] for the temperature induced programmed drug delivery inside the human body. The authors demonstrated that a dual-stimulus (temperature and electric field) responsive system containing conducting polymer polypyrrole nanoparticles can be used to trigger a dosage-controlled release of drugs. Such a study finds use in several important applications such as in designing anticancer medicines. Chaban and co-workers have studied the pressure induced delivery of drugs inside the body[20] and have observed a rapid growth of pressure of water under nanoconfinement over a few degrees above the boiling temperature of water which could be a novel scheme for drug delivery. Similarly, packaged polar drug molecules can be released into tissue from the carbon nanotube heated by the laser.[20] Moreover, nano/micro pumps can be designed based on liquid−vapor phase change under confinement.[21,22] The actuation of the pump is driven by the difference in surface tensions between the confined phases.

External electric and magnetic fields can remarkably affect the properties of fluids. Maerzke and co-workers studied the effects of electric field on vapor−liquid phase transitions of bulk phase systems of water, methanol, and dimethyl ether.[23] They observed an increase in the critical temperature with the electric field for all the fluids. Such effects find applications in several emerging technologies. Electrospinning is one such technology that is used for spinning nanofibers generated by an electrified jet.[24,25] The electrostatic repulsion between charges on nozzle surfaces and evaporation of solvent causes the nanofibers to stretch.

Several experimental studies have been carried out on the effects of the electric field on bulk fluids. Debye and Kleboth studied the effects of an external electric field on a binary mixture of isooctane/nitrobenzene and observed a decrease in the critical temperature with increasing electric field.[26] This decrease in the critical temperature was concluded to be proportional to the square of the applied electric field strength by Orzechowski.[27] Beaglehole also noticed similar effects of the electric field on the critical temperature of a binary mixture of

Special Issue: Modeling and Simulation of Real Systems

Received: February 16, 2014
Accepted: May 22, 2014
Published: June 4, 2014

cyclohexane/aniline.[28] In contrast, Early was unable to find any change in the critical temperature,[29] which was in contradiction to the results of earlier experiments.[26,28] Early attributed the difference to the local heating caused by the applied electric field.[29] Recently, Hegseth and Amara observed an increase in the critical temperature of SF_6 on the application of an electric field.[30]

The effects of an electric field, however, become more convoluted under confinement. Water shows a decrease in its critical temperature with an increase in the electric field under confinement.[31] This behavior is in complete contrast to that of the bulk phase. The behavior could be explained by the mean field theory which predicts a direct dependency of critical temperature on coordination number.[32] As shown by Srivastava et al.,[31] the coordination number decreases under confinement with an increase in electric field, hence resulting in a decrease in the critical temperature. This is also reflected in the reduction in the density of the fluid as seen by Vaitheeswaran et al.[33] for water in hydrophobic confinement under the external electric field. In other words, an electric field enhances the evaporation rate of confined water, which is in contrast to the theory of electrostriction. Bratko et al. studied a similar system to observe the usual phenomenon of electrostriction, i.e., an increase in the density of confined water under an electric field.[34,35] To resolve the above discrepancy England et al.[36] argued that a lower electric field (< 2.0 $V{\cdot}nm^{-1}$) results in a loss of alignment of water molecules due to geometric frustrations leading to a decrease in density. However, higher electric fields (> 6.0 $V{\cdot}nm^{-1}$) align the water molecules along with the field enhancing its density. Recently, the influence of an external magnetic field on nanoconfined water was studied by Zhang et al.,[37], and a new phase of bilayer crystalline ice at a very high freezing point of 340 K was observed. Moreover, the freezing temperature was found to increase with increasing magnetic field.

The anomalous behavior of nanoconfined water under the electric field observed[31] recently is yet to be seen for other polar fluids under confinement. Though some works on confined alcohols have been done,[18,38,39] the effect of the electric field on the vapor−liquid phase equilibria of nanoconfined alcohols is not known. Hence to address the above question, we utilize molecular simulations to study the vapor−liquid equilibria of nanoconfined methanol and ethanol under the external electric field. The rest of the article is organized as follows. In the next section we describe the model and methods employed in this work. Section 3 presents the results and discussions followed by the conclusion in section 4.

2. MODEL AND METHODOLOGY

A TraPPE−UA model, which uses pseudo atoms for each CH_x group, is being used to model methanol and ethanol molecules.[40] Nonbonded interactions are calculated using Lennard−Jones (LJ) and columbic potentials, as per eq 1.

$$U_{nonbonded}(r_{ij}) = 4\varepsilon_{ij}[(\sigma_{ij}/r_{ij})^{12} - (\sigma_{ij}/r_{ij})^{6}] + q_i q_j/4\pi\varepsilon_0 r_{ij} \quad (1)$$

where, r_{ij}, ε_{ij}, σ_{ij}, q_i, and ε_0 are the separation distance, LJ potential well-depth, LJ diameter, partial charges, and dielectric permittivity constant, respectively. The unlike LJ interactions are determined by Lorentz−Berthelot mixing rules as shown in eq 2.

$$\sigma_{ij} = \frac{(\sigma_{ii} + \sigma_{jj})}{2} \text{ and } \varepsilon_{ij} = \sqrt{\varepsilon_{ii}\cdot\varepsilon_{jj}} \quad (2)$$

$$U_{stretching} = \frac{1}{2}k_b(r - r_0)^2 \quad (3)$$

$$U_{bending} = \frac{1}{2}k_\theta(\theta - \theta_0)^2 \quad (4)$$

$$U_{torsion} = c_0 + c_1[1 + \cos(\phi)] + c_2[1 - \cos(2\phi)] + c_3[1 + \cos(3\phi)] \quad (5)$$

$$U_{field} = -\sum_{i=1}^{N}\sum_{j=1}^{3} q_i\cdot(r_{ji}\cdot E) \quad (6)$$

All bonds and angles are modeled using harmonic potentials and are given by eqs 3 and 4 respectively, where k_b and k_θ are force constants, and r, θ, r_0, and θ_0 are bond length, bond angle, and their corresponding equilibrium values, respectively. The OPLS-UA force field is used for the calculation of dihedral interactions, as shown in eq 5. The energy contribution from the applied electric field is calculated using eq 6, where r_{ij} is the position vector of the i^{th} particle along the j^{th} direction. q_i is the charge of the i^{th} particle, and E is the strength of the applied electric field. All the force field parameters are tabulated in Table 1.

Table 1. Force Field Parameters of Alcohols and Graphite Surface

nonbonded	charge	σ (nm)	ε (kcal·mol^{-1})
(C)−C	0.00	0.319	0.000
(CH_3)−O	0.265	0.375	0.1948
(CH_2)−O	0.265	0.395	0.0914
(O)−H	−0.700	0.302	0.1848
(H)−O	0.435	0.000	0.0000
bonds	r_0 (nm)	k_b (kcal·mol^{-1}·nm^{-2})	
C−C	0.1420	46900	
CH_3−CH_2	0.1540	34000	
CH_3−O	0.1430	32000	
O−H	0.0945	55400	
angles	θ (degree)	k_θ (kcal·mol^{-1}·rad^{-2})	
CH_3−CH_2−O	109.47	50	
CH_3−O−H	108.50	55	
CH_2−O−H			
dihedrals	c_0 (K)	c_1 (K)	c_2 (K)	c_3 (K)
CH_3−CH_2−O−H	0.00	209.82	−29.17	187.93

The fluid is confined between the two graphite sheets separated by 4.0 nm in the Z direction. Each graphite sheet consists of two graphene layers, and is placed along the XY plane. The periodic boundary condition is applied along the unbounded directions X and Y. The two-dimensional corrections are employed as per the procedure of Gordillo et al.[41] PPPM (particle−particle particle−mesh) technique is applied for the calculation of long-range interactions. The Nosé−Hoover thermostat is used to maintain the temperature in the system. An integration time of 1 fs is used in all the simulations. The simulations are performed using the LAMMPS MD package.[42] All simulations are carried out in the NVT ensemble (constant number of particles N, volume V, and temperature T). The simulations are equilibrated for a period of 0.5 ns, followed by a production cycle of 0.5 ns. At each temperature, the density profiles are obtained by averaging the two-phase density profiles over appropriate regions. In this study, we have applied an

dx.doi.org/10.1021/je5001582 | J. Chem. Eng. Data 2014, 59, 3090−3097

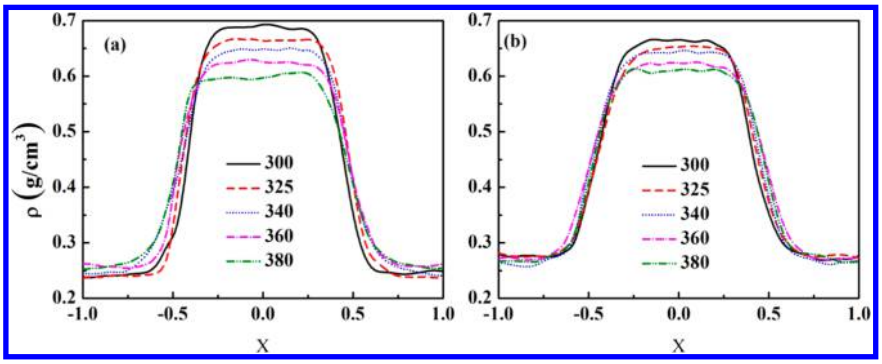

Figure 1. Density profile of vapor and liquid phases of methanol (a) and ethanol (b), under a slit pore of width 4 nm in the absence of an electric field, at different temperatures along the *X*-direction of the system. *Y*-Axis of the plots represents density of the system in real unit, whereas the *X*-axis is the length of the simulation box in the *X*-direction, in reduced unit.

electric field perpendicular to the surface. The electric field, *E*, is varied from 0 V·nm^{-1} to 2.5 V·nm^{-1}. The statistical error in the physical quantities is calculated using the standard deviation of the block-averaged values.

The vapor−liquid critical properties are obtained by fitting the coexistence densities over the range of temperatures according to the law of the rectilinear diameter (eq 7)[43] and the scaling law of density (eq 8).[44]

$$\rho_l - \rho_v = B(1 - T/T_c)^{\beta} \quad (7)$$

$$(\rho_l + \rho_v)/2 = \rho_c + A(1 - T/T_c) \quad (8)$$

where ρ_l, ρ_v, ρ_c, T_c, and β are liquid density, vapor density, critical density, critical temperature, and critical exponent, respectively. *A* and *B* are fitting parameters. The errors in the coexistence densities and critical properties are found to be less than 2 %.

3. RESULTS AND DISCUSSIONS

Figure 1a and b present the density profiles of the vapor−liquid phase coexistence of methanol and ethanol at different temperatures in a slit pore of width 4.0 nm. As the temperature is increased, the density of the liquid phase is lowered, whereas the vapor density increases akin to the behavior seen for the bulk phase.[23] This is more evident for methanol than for ethanol, within the temperature range 300 K to 380 K, as also seen for the bulk phase. The critical temperature and the critical density, evaluated using eq 7, are 13 % lower and 57 % higher than that of the bulk fluid, respectively.[23,45] The corresponding critical exponent β is approximately 0.18 for methanol and ethanol under 4.0 nm slit pore confinement, which is also an indicative of the behavior of the fluids in between the bulk (3D) and 2D fluids.[6]

Figure 2 presents the effect of the external field on the vapor−liquid density profile of methanol under confinement at a typical temperature of 360 K. The electric field reduces the vapor density substantially as clearly seen for the case of E = 1.0 V·nm^{-1}, which reduces the vapor density from 0.253 g·cm^{-3} to 0.235 g·cm^{-3} i.e., approximately 7.1 %. Interestingly, liquid density is also suppressed in the presence of an electric field, though not significantly as compared to the vapor phase. For example, the corresponding reduction in the density at E = 1.0 V·nm^{-1} is 0.5 %. An increase in the electric field further decreases the density of the vapor and liquid phases. The effect of the electric field is more pronounced at lower temperature. For example, at T = 325 K, vapor and liquid densities are

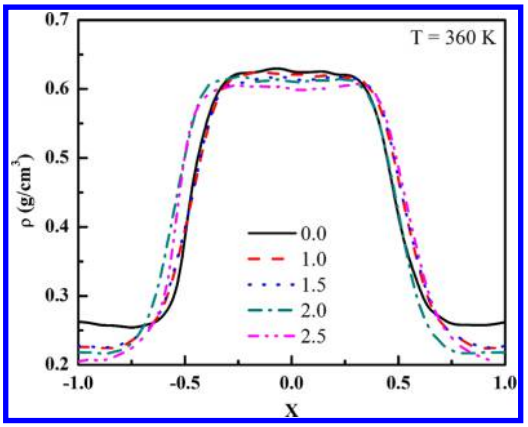

Figure 2. Vapor−liquid density profile of nanoconfined methanol at a temperature of 360 K under varying external electric field in V·nm^{-1}. The axes are similar to those of Figure 1

reduced by ∼8 % and ∼1 %, respectively, at E = 1.0 V·nm^{-1}. The critical temperature and density are also reduced by 7.2 % and 1.2 %, respectively, at E = 1.0 V·nm^{-1}, which is in contrast to the behavior seen for the bulk fluid.[23,45]

Figure 3 illustrates the effects of an external electric field on the vapor−liquid coexistence envelopes of confined methanol and ethanol. Similar to the case of methanol, as shown in Figure 2, vapor and liquid densities of ethanol under confinement decreases with an increase in electric field. However, the vapor−liquid coexistence envelope shrinks or expands depending on the amount of decrease in the saturated liquid and vapor densities under the electric field. This is in contrast to the behavior of the bulk fluid for which the vapor−liquid coexistence envelope broadens in the presence of an electric field.[23] It is observed that the amount of decrease in the vapor phase density is minimal from E = 1.0 V·nm^{-1} to 1.5 V·nm^{-1}. However, the effect is more pronounced in the liquid phase up to E = 1.5 V·nm^{-1}, which is found to reduce relatively more for both nanoconfined methanol and ethanol. This essentially indicates that the vapor−liquid envelope shrinks with increasing E value. Hence, the critical temperature of nanoconfined methanol and ethanol decreases with the electric field. However, this behavior of the critical temperature holds until 1.5 V·nm^{-1}. Beyond 1.5 V·nm^{-1}, the effect of the electric field is relatively more pronounced on the vapor phase compared to the liquid phase. For example, at 360 K, the liquid density decreases by 0.003 g·cm^{-3} (0.5 %) and 0.011 g·cm^{-3} (1.8 %) for E = 2.0 V·nm^{-1} and E = 2.5 V·nm^{-1}, respectively, with respect to the liquid density at E = 1.5 V·nm^{-1};

dx.doi.org/10.1021/je5001582 | J. Chem. Eng. Data 2014, 59, 3090−3097

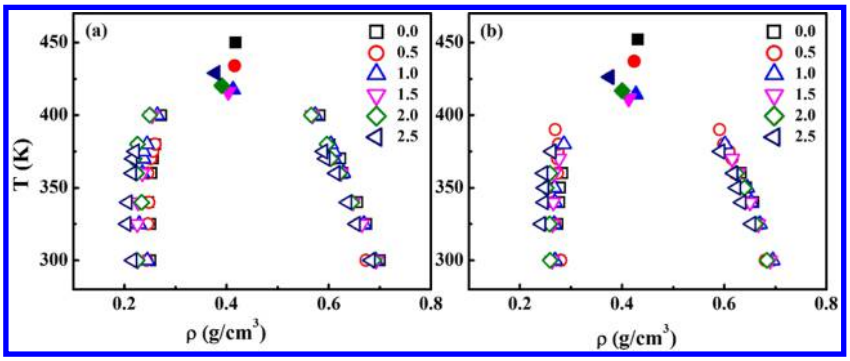

Figure 3. Vapor–liquid coexistence curve of methanol (a) and ethanol (b), confined in graphitic pore of size H = 4 nm at variable electric fields of strength (in V·nm^{-1}): squares, E = 0.0; circles, E = 0.5; triangles, E = 1.0; inverse triangles, E = 1.5; diamonds, E = 2.0; and left triangle, E = 2.5. Filled symbols represent the critical points, respectively.

Table 2. Vapor–Liquid Equilibrium Data for Methanol in Confined Graphitic Slit Pore of 4.0 nm under Variable External Electric Field[a]

	density, ρ/g·cm^{-3} [at E = 0.00 V·nm^{-1}]			density, ρ/g·cm^{-3} [at E = 0.5 V·nm^{-1}]			density, ρ/g·cm^{-3} [at E = 1.0 V·nm^{-1}]	
T (K)	liquid	vapor	T (K)	liquid	vapor	T (K)	liquid	vapor
300	0.700(3)	0.251(9)	300	0.673(4)	0.244(4)	300	0.692(5)	0.245(8)
325	0.674(4)	0.251(5)	325	0.658(6)	0.246(9)	325	0.669(4)	0.229(3)
340	0.656(1)	0.247(6)	340	0.642(5)	0.248(4)	360	0.629(2)	0.235(7)
360	0.627(4)	0.253(9)	360	0.622(2)	0.246(5)	370	0.614(4)	0.253(5)
370	0.623(3)	0.256(11)	370	0.610(7)	0.252(14)	375	0.610(5)	0.238(8)
380	0.602(5)	0.260(9)	375	0.604(4)	0.256(8)	380	0.604(3)	0.257(6)
400	0.582(5)	0.272(12)	380	0.600(2)	0.260(6)	400	0.573(5)	0.264(10)
450(3)	0.418(4)		434(10)	0.416(5)		418(5)	0.413(6)	
	density, ρ/g·cm^{-3} [at E = 1.50 V·nm^{-1}]			density, ρ/g·cm^{-3} [at E = 2.0 V·nm^{-1}]			density, ρ/g·cm^{-3} [at E = 2.5 V·nm^{-1}]	
T (K)	liquid	vapor	T (K)	liquid	vapor	T (K)	liquid	vapor
300	0.693(4)	0.226(8)	300	0.689(5)	0.225(8)	300	0.682(4)	0.216(9)
325	0.665(5)	0.225(5)	340	0.645(5)	0.234(11)	325	0.653(5)	0.204(5)
340	0.647(4)	0.227(6)	360	0.621(5)	0.223(6)	340	0.636(4)	0.206(10)
360	0.624(7)	0.235(8)	370	0.604(4)	0.219(11)	360	0.613(7)	0.215(6)
400	0.568(8)	0.254(8)	380	0.597(3)	0.226(6)	370	0.594(8)	0.216(14)
416(4)	0.403(7)		400	0.566(7)	0.250(7)	375	0.589(5)	0.221(10)
			420(3)	0.391(2)		429(3)	0.378(9)	

[a]The numbers in parentheses indicate the 67 % confidence limits of the last digit of the reported value.

whereas, corresponding changes in the vapor density are 0.012 g·cm^{-3} (5 %) and 0.020 g·cm^{-3} (8 %) at E = 2.0 V·nm^{-1} and 2.5 V·nm^{-1}, respectively. Hence, beyond 1.5 V·nm^{-1} we observe broadening in the vapor–liquid coexistence envelope, which essentially increases the critical temperature. On the other hand, critical density monotonically decreases with increasing electric field. Tables 2 and 3 summarize the values of vapor–liquid coexistence densities for methanol and ethanol, respectively.

The layering of the fluids on the surface can be observed from the z-density profiles of ethanol and methanol at a typical temperature of 360 K, which is shown in Figure 4. It is evident that significant layering is present in the liquid and vapor phases of nanoconfined ethanol and methanol. The number of layers in the liquid and vapor phases is three and two, respectively. The density of the contact layer in the liquid phase is approximately 2 g·cm^{-3}, for both methanol and ethanol; whereas, in the case of the vapor phase, the contact layer density is approximately 1 g·cm^{-3}. The density in the liquid phase beyond the three layers is constant at around 0.638 g·cm^{-3} and 0.633 g·cm^{-3}, for methanol and ethanol, respectively. On the other hand, vapor density decays to zero after a distance of 1.5 nm from the surface. The density of the fluid in the layer adjacent to the surface increases with the increase in electric field at a constant temperature for both liquid and vapor phases, though the change in the vapor phase density is on the order of 1 %, and that of the liquid phase is approximately 10 %. However, overall vapor and liquid phase densities are reduced due to the decrease in the density away from the contact layer, which is more visible in the vapor phase, as evident in Figure 4.

Figure 5 shows a plot of critical temperatures vs the electric field for methanol and ethanol. Table 4 summarizes the critical properties of nanoconfined methanol and ethanol under different electric fields. It is evident from the figure that the change in critical temperature is quadratic in nature. With increasing electric field, the critical temperature reduces until a strength of 1.5 V·nm^{-1}, beyond which it increases. In the absence of an external electric field, the ethanol shows a higher critical temperature than that of methanol, as expected. However, under the applied electric field the behavior of the critical temperature reverses. As the electric field increases, the critical

dx.doi.org/10.1021/je5001582 | J. Chem. Eng. Data 2014, 59, 3090–3097

Table 3. Vapor−Liquid Equilibrium Data for Ethanol in Confined Graphitic Slit Pore of 4.0 nm under Variable Electric Field[a]

	density, ρ/g·cm^{-3} [at E = 0.00 V·nm^{-1}]			density, ρ/g·cm^{-3} [at E = 0.5 V·nm^{-1}]			density, ρ/g·cm^{-3} [at E = 1.0 V·nm^{-1}]	
T (K)	liquid	vapor	T (K)	liquid	vapor	T (K)	liquid	vapor
300	0.689(6)	0.277(5)	325	0.661(4)	0.268(6)	300	0.695(5)	0.269(4)
325	0.665(4)	0.274(7)	340	0.643(3)	0.265(8)	325	0.670(5)	0.267(12)
340	0.657(3)	0.277(7)	360	0.621(6)	0.274(6)	340	0.653(2)	0.268(8)
350	0.643(5)	0.279(12)	370	0.617(6)	0.273(10)	350	0.645(6)	0.267(4)
360	0.633(3)	0.283(8)	380	0.599(10)	0.276(12)	380	0.601(3)	0.286(7)
452(3)	0.431(4)		437(10)	0.420(9)		414(4)	0.413(3)	
	density, ρ/g·cm^{-3} [at E = 1.5 V·nm^{-1}]			density, ρ/g·cm^{-3} [at E = 2.0 V·nm^{-1}]			density, ρ/g·cm^{-3} [at E = 2.5 V·nm^{-1}]	
T (K)	liquid	vapor	T (K)	liquid	vapor	T (K)	liquid	vapor
300	0.690(3)	0.263(5)	300	0.684(3)	0.259(8)	325	0.653(8)	0.242(11)
325	0.667(6)	0.264(13)	325	0.661(7)	0.258(10)	340	0.634(8)	0.247(13)
340	0.651(6)	0.265(8)	350	0.639(4)	0.244(10)	350	0.624(9)	0.235(7)
360	0.628(5)	0.267(7)	360	0.624(8)	0.259(8)	360	0.618(7)	0.235(9)
370	0.616(4)	0.267(8)				375	0.592(9)	0.262(7)
412(3)	0.413(9)		417(2)	0.400(8)		426(3)	0.376(3)	

[a]The numbers in parentheses indicate the 67 % confidence limits of the last digit of the reported value.

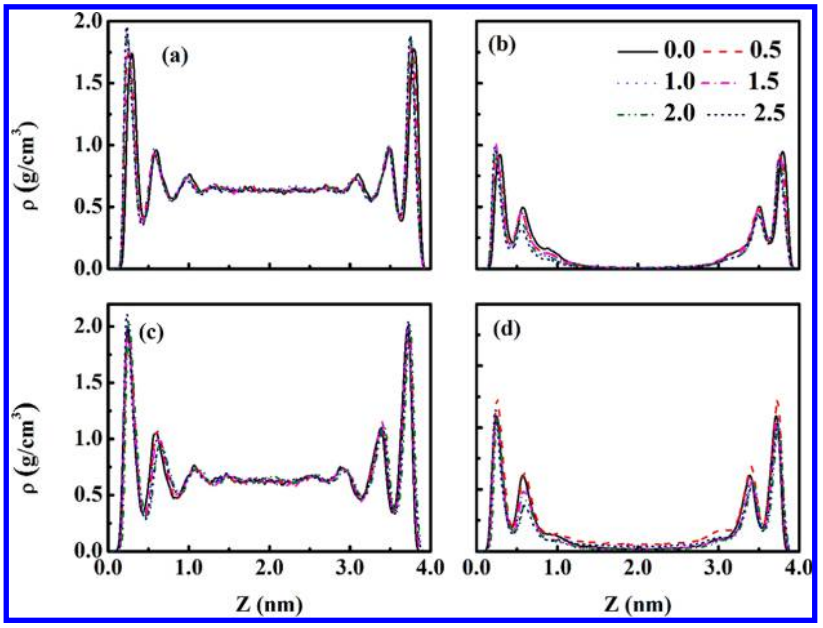

Figure 4. Density profiles of liquid phase (left panels) and vapor phase (right panels) of the nanoconfined methanol (top panels) and ethanol (bottom panels), across the width of the graphite slit pore, under varying electric field at a temperature of 360 K.

temperatures of the methanol become higher than that of ethanol. The difference is maximum at E = 1.5 V·nm^{-1}, at the minimum critical temperature. However, with a further increase in the electric field, the critical temperature of ethanol approaches the value of methanol as can be seen for the case of E = 2.5 V·nm^{-1}. In order to understand the reason for ethanol to behave unusually, we consider a typical temperature of 340 K to observe the effect of the electric field and the ethyl group on the densities, with respect to the case for E = 0.0 V·nm^{-1}. The vapor-like phase of confined ethanol has a significantly higher density compared to that of confined methanol, due to the effect of the surface and the additional methyl group. With a high density in the vapor phase, the cohesive energy per particle is also higher in the ethanol vapor phase, making the vapor phase of the methanol relatively more responsive to the external field. The effect of the preferential wetting on the surface by the alkyl group is hardly seen in the critical temperature difference between the two fluids at zero electric field. However, with an increase in the electric field from E = 0.0 V·nm^{-1} to E = 1.5 V·nm^{-1}, due to the responsive vapor phase of methanol, the vapor phase density is reduced by 8 % as opposed to 4 % in ethanol. This primarily leads to the higher difference between the vapor and liquid densities in the case of methanol. This essentially means a higher temperature is needed to make the two phases indistinguishable leading to relatively higher critical temperature for the confined methanol compared to the confined ethanol.

In order to understand the behavior of critical temperature, we calculated the radial distribution function, $g(r)$, of the liquid phase of confined methanol and ethanol. Though $g(r)$ is not

dx.doi.org/10.1021/je5001582 | J. Chem. Eng. Data 2014, 59, 3090−3097

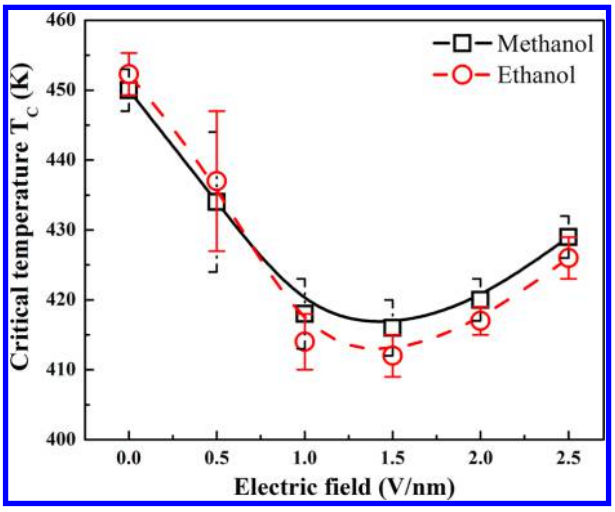

Figure 5. Critical temperature, T_c, of confined methanol and ethanol in a graphitic pore of width 4.0 nm, against variable electric fields.

Table 4. Critical Temperature, T_c, and Density, ρ_c, of Methanol and Ethanol in Graphitic Slit Pore of Thickness 4.0 nm under External Electric Field, E[a]

	methanol		ethanol	
E	T_c	ρ_c	T_c	ρ_c
V·nm^{-1}	K	g·cm^{-3}	K	g·cm^{-3}
0.00	450(3)	0.418(4)	452(3)	0.431(4)
0.50	434(10)	0.416(5)	437(10)	0.420(9)
1.00	418(5)	0.413(6)	414(4)	0.413(3)
1.50	416(4)	0.403(7)	412(3)	0.413(9)
2.00	420(3)	0.391(2)	417(2)	0.400(8)
2.50	429(3)	0.378(9)	426(3)	0.376(3)

[a]The numbers in parentheses indicate the 67 % confidence limits of the last digit of the reported value.

affected significantly by the electric field, the integral of the radial distribution function, i.e. the overall coordination number, $N(r)$ values in the liquid phase for both methanol and ethanol are found to vary with electric field, as shown in Figure 6. Interestingly, $N(r)$ does not change much in the presence of the electric field until the first coordination shell. However, the difference is clearly observed at a higher distance. It is clear from the plot that the coordination number decreases up to E = 1.5 V·nm^{-1}. For E higher than 1.5 V·nm^{-1}, $N(r)$ is found to increase beyond the first coordination shell, for both methanol and ethanol. The mean field theory[32] states that

$$T_c = cz\varepsilon/k_B \tag{9}$$

where T_c is the critical temperature, c is a constant, z is the coordination number for a molecule in the fluid, ε is the energy of interaction with the nearest-neighbor molecule, and k_B is Boltzmann's constant. As per the theory a decrease in the coordination number up to an electric field strength of 1.5 V·nm^{-1} predicts a decrease in the critical temperature. A further increase in the electric field, E > 1.5 V·nm^{-1}, increases the coordination number, and so does the critical temperature. Hence, the mean field theory correctly predicts the behavior of the critical temperature of nanoconfined polar fluids under the influence of the electric field. In order to understand the effect of the electric field on the orientation of methanol and ethanol molecules under confinement, we investigated the order parameter (S), defined as

$$S = \frac{1}{2}\langle(3\cos^2\theta - 1)\rangle \tag{10}$$

where θ is the angle between the electric field and the end-to-end vector. It is evident from this expression that when the molecules are parallel or antiparallel to the field, i.e., $\theta \in 0°$, 180°, S = 1. For the case when molecules are perpendicular to the field, i.e., θ = 90°, S tends toward −0.5. In the random alignment of molecules, S should approach 0.

Figure 7 shows the order parameter of different phases against several temperatures for E ranging from 0 V·nm^{-1} to 2.5 V·nm^{-1}. The order parameter values are very small which indicates a weak dependency of molecular arrangement on the electric field. Figure 7a shows the variation of the order parameter of methanol molecules within the liquid phase. The order parameter value increases slowly with increasing temperature indicative of enhanced randomness at higher temperatures. However, the value decreases with an increase in the electric field. The order parameter value drops further when the electric field is higher than 1.5 V·nm^{-1}. Lower values of the order parameter indicate that the molecules tend to align along the electric field. On the other hand, for the vapor phase, the order parameter does not show any significant effect with electric field at lower temperature (see Figure 7b). However, the effect of the electric field is slightly visible at higher temperature, where molecules orient toward the electric field at a higher electric field. In the case of ethanol molecules, the order parameter in the liquid phase is relatively irresponsive to the

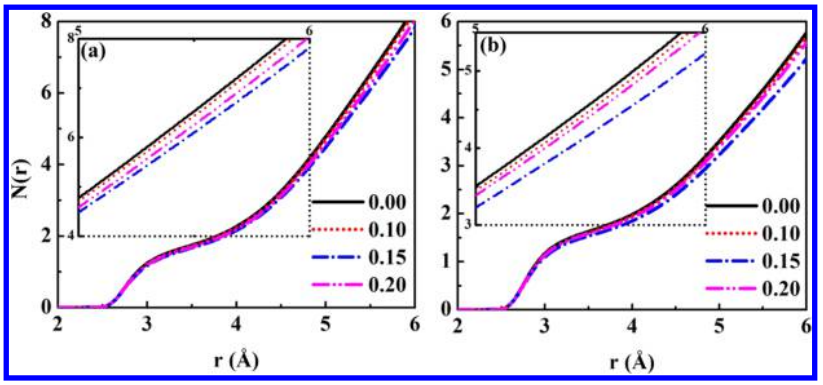

Figure 6. Overall coordination number $N(r)$ of the liquid phase at variable electric fields in V·nm^{-1}, for methanol (a) and ethanol (b). Insets show closer view of coordination number near the first coordination shell.

dx.doi.org/10.1021/je5001582 | J. Chem. Eng. Data 2014, 59, 3090−3097

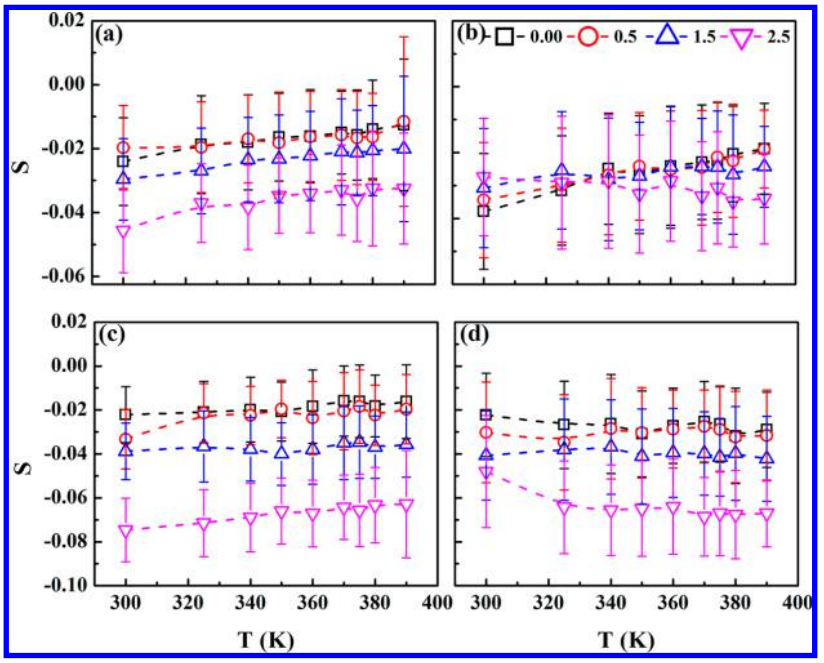

Figure 7. Order parameter S of liquid phase (left panels) and vapor phase (right panels) confined in graphitic pore of width H = 4.0 nm against temperature for variable electric fields in V·nm^{-1}, for methanol (top panels) and ethanol (bottom panels). The lines are to guide the eye.

temperature (see Figure 7c) as clearly seen for E = 1.5 V·nm^{-1}. However, alcohol molecules tend to orient more along the electric field at higher E values. In the vapor phase, the behavior of ethanol molecules is more or less similar to that seen for the methanol. However, it should be noted that the errors in the order-parameter values are high due to the competing effects of the surface and electric field. Nevertheless, the order parameter approaches the zero value line with the continuous increase in the temperature, as expected due to the increase in the thermal fluctuations with increasing temperature favoring a more random alignment of the molecules.

4. CONCLUSION

We have studied the vapor−liquid phase transitions of methanol and ethanol confined in graphitic slit pores of size H = 4.0 nm under variable electric field strengths (0.0, 1.0, 1.5, 2.0, and 2.5) V·nm^{-1}. The electric field is found to reduce the critical temperature of the nanoconfined methanol and ethanol up to a field strength of 1.5 V·nm^{-1}, and thereafter the critical temperature increases for both methanol and ethanol with increasing electric field. The critical density is found to decrease with increasing electric field. We have also investigated the coordination number $N(r)$, in the liquid phase, of confined methanol and ethanol under electric fields. It is found that $N(r)$ decreases up to a field strength of 1.5 V·nm^{-1} and increases thereafter for both methanol and ethanol. This explains the observed trend in the critical temperature as per the mean field theory.

AUTHOR INFORMATION

Corresponding Author

*E-mail: jayantks@iitk.ac.in.

Notes

The authors declare no competing financial interest.

ACKNOWLEDGMENTS

This work is supported by the Department of Science and Technology (DST), Government of India. Computational resources are provided by the Centre for Development and Advance Computing (CDAC) Pune, India, and HPC Centre of Indian Institute of Technology Kanpur.

REFERENCES

(1) Ronen, Z. Water Confined to a Slab Geometry: A Review of Recent Computer Simulation Studies. *J. Phys.: Condens. Matter* **2004**, *16*, S5371.

(2) Koga, K.; Gao, G. T.; Tanaka, H.; Zeng, X. C. Formation of Ordered Ice Nanotubes inside Carbon Nanotubes. *Nature* **2001**, *412*, 802−805.

(3) Cummings, P. T.; Docherty, H.; Iacovella, C. R.; Singh, J. K. Phase Transitions in Nanoconfined Fluids: The Evidence from Simulation and Theory. *AIChE J.* **2010**, *56*, 842−848.

(4) Hummer, G.; Rasaiah, J. C.; Noworyta, J. P. Water Conduction through the Hydrophobic Channel of a Carbon Nanotube. *Nature* **2001**, *414*, 188−190.

(5) Ivan, B.; Alfons, G.; Alla, O. Water in Nanopores: II. The Liquid−Vapour Phase Transition near Hydrophobic Surfaces. *J. Phys.: Condens. Matter* **2004**, *16*, S5345.

(6) Singh, S. K.; Singh, J. K.; Kwak, S. K.; Deo, G. Phase Transition and Crossover Behavior of Colloidal Fluids under Confinement. *Chem. Phys. Lett.* **2010**, *494*, 182−187.

(7) Sliwinska-Bartkowiak, M.; Sikorski, R.; Sowers, S. L.; Gelb, L. D.; Gubbins, K. E. Phase Separations for Mixtures in Well-Characterized Porous Materials: Liquid−Liquid Transitions. *Fluid Phase Equilib.* **1997**, *136*, 93−109.

(8) Huang, H. C.; Chen, W. W.; Singh, J. K.; Kwak, S. K. Direct Determination of Fluid-Solid Coexistence of Square-Well Fluids Confined in Narrow Cylindrical Hard Pores. *J. Chem. Phys.* **2010**, *132*, 224504.

(9) Srivastava, R.; Docherty, H.; Singh, J. K.; Cummings, P. T. Phase Transitions of Water in Graphite and Mica Pores. *J. Phys. Chem. C* **2011**, *115*, 12448−12457.

(10) Liu, Y.; Panagiotopoulos, A. Z.; Debenedetti, P. G. Finite-Size Scaling Study of the Vapor-Liquid Critical Properties of Confined

Fluids: Crossover from Three Dimensions to Two Dimensions. *J. Chem. Phys.* **2010**, *132*, 144107.
(11) Singh, S. K.; Singh, J. K. Effect of Pore Morphology on Vapor−Liquid Phase Transition and Crossover Behavior of Critical Properties from 3d to 2d. *Fluid Phase Equilib.* **2011**, *300*, 182−187.
(12) Singh, S. K.; Saha, A. K.; Singh, J. K. Molecular Simulation Study of Vapor−Liquid Critical Properties of a Simple Fluid in Attractive Slit Pores: Crossover from 3d to 2d. *J. Phys. Chem. B* **2010**, *114*, 4283−4292.
(13) Long, Y.; Śliwińska-Bartkowiak, M.; Drozdowski, H.; Kempiński, M.; Phillips, K. A.; Palmer, J. C.; Gubbins, K. E. High Pressure Effect in Nanoporous Carbon Materials: Effects of Pore Geometry. *Colloids Surface A* **2013**, *437*, 33−41.
(14) Zheng, M.; et al. Structure-Based Carbon Nanotube Sorting by Sequence-Dependent DNA Assembly. *Science* **2003**, *302*, 1545−1548.
(15) Liu, C.; Fan, Y. Y.; Liu, M.; Cong, H. T.; Cheng, H. M.; Dresselhaus, M. S. Hydrogen Storage in Single-Walled Carbon Nanotubes at Room Temperature. *Science* **1999**, *286*, 1127−1129.
(16) Sholl, D. S.; Johnson, J. K. Making High-Flux Membranes with Carbon Nanotubes. *Science* **2006**, *312*, 1003−1004.
(17) Newsome, D. A.; Sholl, D. S. Influences of Interfacial Resistances on Gas Transport through Carbon Nanotube Membranes. *Nano Lett.* **2006**, *6*, 2150−2153.
(18) Shao, Q.; Huang, L.; Zhou, J.; Lu, L.; Zhang, L.; Lu, X.; Jiang, S.; Gubbins, K. E.; Zhu, Y.; Shen, W. Molecular Dynamics Study on Diameter Effect in Structure of Ethanol Molecules Confined in Single-Walled Carbon Nanotubes. *J. Phys. Chem. C* **2007**, *111*, 15677−15685.
(19) Ge, J.; Neofytou, E.; Cahill, T. J.; Beygui, R. E.; Zare, R. N. Drug Release from Electric-Field-Responsive Nanoparticles. *ACS Nano* **2011**, *6*, 227−233.
(20) Chaban, V. V.; Prezhdo, O. V. Water Boiling inside Carbon Nanotubes: Toward Efficient Drug Release. *ACS Nano* **2011**, *5*, 5647−5655.
(21) Bergstrom, P. L.; Jin, J.; Yu-Ning, L.; Kaviany, M.; Wise, K. D. Thermally Driven Phase-Change Microactuation. *J. Microelectromech S* **1995**, *4*, 10−17.
(22) Liwei, L.; Pisano, A. P.; Lee, A. P. In *Microbubble Powered Actuator*, Solid-State Sensors and Actuators, 1991. Digest of Technical Papers, TRANSDUCERS '91., 1991 International Conference on, 24−27 June 1991; 1991; pp 1041−1044.
(23) Maerzke, K. A.; Siepmann, J. I. Effects of an Applied Electric Field on the Vapor−Liquid Equilibria of Water, Methanol, and Dimethyl Ether. *J. Phys. Chem. B* **2010**, *114*, 4261−4270.
(24) Okuno, Y.; Minagawa, M.; Matsumoto, H.; Tanioka, A. Simulation Study on the Influence of an Electric Field on Water Evaporation. *THEOCHEM* **2009**, *904*, 83−90.
(25) Li, D.; Xia, Y. Electrospinning of Nanofibers: Reinventing the Wheel? *Adv. Mater.* **2004**, *16*, 1151−1170.
(26) Debye, P.; Kleboth, K. Electrical Field Effect on the Critical Opalescence. *J. Chem. Phys.* **1965**, *42*, 3155−3162.
(27) Orzechowski, K. Electric Field Effect on the Upper Critical Solution Temperature. *Chem. Phys.* **1999**, *240*, 275−281.
(28) Beaglehole, D. The Liquid−Vapor Interface of a Binary Liquid Mixture. *J. Chem. Phys.* **1981**, *75*, 1544−1550.
(29) Early, M. D. Dielectric Constant Measurements near the Critical Point of Cyclohexane−Aniline. *J. Chem. Phys.* **1992**, *96*, 641−647.
(30) Hegseth, J.; Amara, K. Critical Temperature Shift in Pure Fluid SF_6 Caused by an Electric Field. *Phys. Rev. Lett.* **2004**, *93*, 057402.
(31) Srivastava, R.; Singh, J. K.; Cummings, P. T. Effect of Electric Field on Water Confined in Graphite and Mica Pores. *J. Phys. Chem. C* **2012**, *116*, 17594−17603.
(32) Givens, J. A.; Stell, G. *Condensed Matter Theories*; Plenum: New York, 1993; Vol. *8*, p 395.
(33) Vaitheeswaran, S.; Yin, H.; Rasaiah, J. C. Water between Plates in the Presence of an Electric Field in an Open System. *J. Phys. Chem. B* **2005**, *109*, 6629−6635.
(34) Bratko, D.; Daub, C. D.; Luzar, A. Field-Exposed Water in a Nanopore: Liquid or Vapour? *Phys. Chem. Chem. Phys.* **2008**, *10*, 6807−6813.
(35) Bratko, D.; Daub, C. D.; Leung, K.; Luzar, A. Effect of Field Direction on Electrowetting in a Nanopore. *J. Am. Chem. Soc.* **2007**, *129*, 2504−2510.
(36) England, J. L.; Park, S.; Pande, V. S. Theory for an Order-Driven Disruption of the Liquid State in Water. *J. Chem. Phys.* **2008**, *128*, 044503.
(37) Zhang, G.; Zhang, W.; Dong, H. Magnetic Freezing of Confined Water. *J. Chem. Phys.* **2010**, *133*, 134703.
(38) Mugele, F.; Baldelli, S.; Somorjai, G. A.; Salmeron, M. Structure of Confined Films of Chain Alcohols. *J. Phys. Chem. B* **2000**, *104*, 3140−3144.
(39) Wang, J.; Li, Z.; Yoon, R.-H.; Eriksson, J. C. Surface Forces in Thin Liquid Films of n-Alcohols and of Water−Ethanol Mixtures Confined between Hydrophobic Surfaces. *J. Colloid Interface Sci.* **2012**, *379*, 114−120.
(40) Chen, B.; Potoff, J. J.; Siepmann, J. I. Monte Carlo Calculations for Alcohols and Their Mixtures with Alkanes. Transferable Potentials for Phase Equilibria. 5. United-Atom Description of Primary, Secondary, and Tertiary Alcohols. *J. Phys. Chem. B* **2001**, *105*, 3093−3104.
(41) Gordillo, M. C.; Nagy, G.; Martí, J. Structure of Water Nanoconfined between Hydrophobic Surfaces. *J. Chem. Phys.* **2005**, *123*, 054707.
(42) Plimpton, S. Fast Parallel Algorithms for Short-Range Molecular Dynamics. *J. Comput. Phys.* **1995**, *117*, 1−19.
(43) Van Poolen, L. J.; Holcomb, C. D.; Niesen, V. G. Critical Temperature and Density from Liquid−Vapor Coexistence Data: Application to Refrigerants R32, R124, and R152a. *Fluid Phase Equilib.* **1997**, *129*, 105−111.
(44) Vega, L.; de Miguel, E.; Rull, L. F.; Jackson, G.; McLure, I. A. Phase Equilibria and Critical Behavior of Square−Well Fluids of Variable Width by Gibbs Ensemble Monte Carlo Simulation. *J. Chem. Phys.* **1992**, *96*, 2296−2305.
(45) Khare, R.; Sum, A. K.; Nath, S. K.; de Pablo, J. J. Simulation of Vapor−Liquid Phase Equilibria of Primary Alcohols and Alcohol−Alkane Mixtures. *J. Phys. Chem. B* **2004**, *108*, 10071−10076.